Alloy decomposition and surface instabilities in thin films

François Léonard and Rashmi C. Desai
Department of Physics, University of Toronto, Toronto, Ontario, Canada M5S 1A7
(Received 14 July 1997; revised manuscript received 16 October 1997)

We show that in the presence of substrate misfit and compositional stresses, static or growing films that undergo surface spinodal decomposition are always unstable to perturbations around the planar surface. For sufficiently rapid deposition processes, the planar surface can be stabilized due to a suppression of the alloy decomposition. Films grown outside of the miscibility gap can become unstable due to the mismatch with the substrate and compositionally generated stresses. We also demonstrate that the instability is independent of the sign of the misfit when the elastic moduli of the alloy constituents are equal, and the existence of a maximum misfit above which the film is always unstable, even at high growth rates. The symmetry under sign reversal of the misfit can be broken by composition-dependent elastic constants. [S0163-1829(98)05508-8]

I. INTRODUCTION

Growing good-quality thin solid layers is an important technological process. Constraints on operating conditions and performance of electronic and optical devices have led to an increase in the complexity of thin films that are being grown. For example, the tailoring of the electronic band gap of semiconductor films can be accomplished by growing *alloy* layers. Although the alloy composition can be tuned to obtain a desirable band gap, the resulting device is useful only if the alloy composition remains homogeneous. Recently, however, there have been experimental reports of composition modulations that appear while the film is growing.[1] Theoretical investigations[2–4] have shown that a possible explanation for these experiments is the presence of phase separation of the alloy constituents at the surface. The composition gradients generated at the surface are then buried in the bulk of the thin film because of the constant deposition of material. Since bulk diffusion is negligible, there is a characteristic length scale for the composition modulations originating from the competition between the phase separation and the deposition of material, and a topview of the film shows lamellar composition patterns for equal volume fractions of the two species. In the absence of elastic effects,[2,3] modulations of the surface profile occur because at the surface, atoms of different species prefer to increase the surface roughness rather than being next to each other. In the absence of a substrate/film misfit but with elastic fields originating from a dependence of the elastic moduli on composition,[4] the lamellar phase can become unstable to the formation of a droplet phase, consisting of hard domains in a soft matrix. Hence, stress and strain effects are crucial in determining the composition profile of the alloy layer.

The effects of a substrate misfit on the surface of a single component film lead to an instability of the planar surface. This instability is responsible for the formation of mounds or islands where elastic relaxation occurs at the peaks, in competition with the extra surface energy. Such instabilities have been observed experimentally[5–7] and predicted theoretically[8–10] by several authors. For alloy layers, the lattice constant and the elastic moduli of the two components can be different, and an interesting coupling arises between the misfit stress and the stress generated by composition inhomogeneities, as shown by Guyer and Voorhees.[11] These authors, however, considered the surface composition to be in equilibrium with a vapor, a strong approximation that neglects the dynamics of phase segregation. Another approach has been proposed by Tersoff[12] based on a step-flow growth model. Experiments correlating the compositional and surface profiles have been recently presented.[13,14]

In this paper, we consider the case where the alloy inhomogeneities are initially induced by thermodynamics alone: the alloy is immiscible at the growth temperature and composition. We also consider the case where the alloy is grown outside of the miscibility gap. Furthermore, the full nonequilibrium nature of the dynamics of phase separation and surface diffusion are taken into account, leading to results that are very different from those in Ref. 11. In particular, we find that the stability is independent of the sign of the misfit when the elastic moduli of the alloy components are equal, and that alloy decomposition is always accompanied by a surface instability. In Sec. II, we introduce the continuum model for the alloy thin film, and in Sec. III, we describe the linear stability analysis. Equations (38) and (39) form one of the central parts of this work. Results are presented for a static film in Sec. IV and for a growing film in Sec. V. The effects of a composition-dependent Young's modulus are discussed in Sec. VI and our conclusion is presented in Sec. VII.

II. MODEL

The substrate is a semi-infinite isotropic solid occupying the space $z<0$, and the film is in the region $0<z \leqslant h(x,y,t)$. The film is composed of two species, corresponding to a binary or pseudobinary alloy, with both species simultaneously deposited by a directed beam. The instantaneous average composition of the alloy film is the same as the composition in the beam, which remains constant in time. The surface $z=0$ separating the substrate from the film is assumed to remain flat and coherent. Furthermore, the interactions of the film with the substrate are symmetric for the components of the film, and are assumed not to affect the surface energy. A neutral substrate has been shown to produce droplets of both phases of the film in contact with the

substrate.[3] An essential ingredient in our model is that diffusion of material proceeds along the surface only, since bulk diffusion coefficients are typically much smaller than surface diffusion coefficients. The neglect of bulk diffusion means that the composition profile in the z direction can be obtained from the history of the composition at the surface. In this section, the elastic constants (Young's modulus E, shear modulus μ, and Poisson ratio ν) of the substrate and of the film are assumed to be equal and independent of the composition.

The composition of the film is described by a continuous variable $\phi(\mathbf{r})$ proportional to the local composition difference of the two constituents: for example, for an alloy of type A_xB_{1-x}, $\phi=1$ corresponds to $x=0$, $\phi=-1$ to $x=1$ and $\phi=0$ to $x=1/2$. The important effects in heteroepitaxy arise because the lattice constants of the film components are different: the lattice constant of the film a_f depends on ϕ through the relation $\ln a_f=\eta\phi$, defining the solute expansion coefficient $\eta=(\partial a_f/\partial\phi)/a_f$. The misfit between the substrate and the film is $\varepsilon=(a_f-a_s)/a_s$, ($a_s$ is the lattice constant of the substrate); $\varepsilon>0$ implies that the film is compressively strained.

The free energy of the system consists of three parts: a contribution from the elastic energy, a contribution due to the thermodynamics of the binary alloy, and a term that represents the surface energy. The total free-energy functional is written as

$$\mathcal{F}[\phi,\mathbf{u},h]=\mathcal{F}_{\rm el}[\phi,\mathbf{u},h]+\mathcal{F}_{\rm GL}[\phi,h]+\mathcal{F}_s[h], \tag{1}$$

where $\mathcal{F}_{\rm el}$ is the elastic free-energy functional, $\mathcal{F}_{\rm GL}$ is the Ginzburg-Landau free-energy functional that represents the thermodynamics, and $\mathcal{F}_s$ is the surface free-energy functional. Here, $\mathbf{u}(\mathbf{r})$ is the displacement vector representing displacements from the local equilibrium position and is related to the strain tensor through $\mu_{ij}=(\nabla_i u_j+\nabla_j u_i)/2$, with the indices i and j equal to x,y or z. Because the elastic fields will cause deformations to extend into the substrate, the elastic term has to be calculated over the whole system:

$$\mathcal{F}_{\rm el}[\phi,\mathbf{u},h]=\frac{1}{2}\int_{-\infty}^{h}d^3r S_{ijkl}\sigma_{ij}\sigma_{kl}, \tag{2}$$

with S_{ijkl} the elastic compliance tensor and σ_{ij} the stress tensor. For isotropic bodies, $S_{ijkl}=\delta_{ik}\delta_{jl}(1+\nu)/E-\delta_{ij}\delta_{kl}\nu/E$ (δ_{ij} is the Kronecker delta). The essential properties of the binary compound phase behavior is captured by the Ginzburg-Landau energy,

$$\mathcal{F}_{\rm GL}[\phi,h]=\int_0^h d^3r\left[-\frac{r'}{2}\phi^2+\frac{u}{4}\phi^4+\frac{c}{2}|\nabla\phi|^2\right]. \tag{3}$$

This coarse-grained free-energy functional comprises contributions from the internal energy and from the entropy. The constant r' is proportional to T_c-T, where T_c is the critical temperature of the binary alloy. When $T>T_c$, minimization of the free energy shows that there exists only one solution for ϕ, i.e., $\phi=0$, corresponding to a homogeneously mixed system. When $T<T_c$, the first two terms have a double-well structure, with minima at $\phi_\pm=\pm\sqrt{r'/u}$, and the range of ϕ between ϕ_+ and ϕ_- represents the coexistence region of the phase diagram. The term proportional to $|\nabla\phi|^2$ penalizes gradients in ϕ, and its coefficient c is proportional to the square of the characteristic interfacial length scale. In this paper, we assume that the substrate is held at a constant temperature below or above the critical temperature of the alloy layer, and that thermal equilibrium is immediately reached upon contact with the substrate. The last contribution in the total free-energy functional is the surface energy,

$$\mathcal{F}_s[h]=\gamma\int d^2r\sqrt{g}, \tag{4}$$

with γ the surface tension and $g=1+|\nabla h|^2$ the determinant of the surface metric. Here, we consider simplified cases where the surface tension is isotropic and independent of the composition or the displacement vector.

The boundary conditions for the system are as follows. For molecular-beam-epitaxy (MBE) growth, the pressure above the film is negligible; hence the total force on a mass element on the surface is zero. This implies that

$$\sigma^f_{ij}n_j=0 \quad \text{at} \quad z=h, \tag{5}$$

with the unit vector $\mathbf{n}=(-\nabla h,1)/\sqrt{g}$ oriented towards the half-space of the positive z direction. Because the plane $z=0$ remains flat and coherent, the displacement vector and the stress tensor must be continuous there, implying that

$$\sigma^f_{zi}=\sigma^s_{zi} \quad \text{and} \quad \mathbf{u}^f=\mathbf{u}^s \quad \text{at} \quad z=0. \tag{6}$$

Also, we require the displacement vector within the substrate to vanish far from the film/substrate interface: $\mathbf{u}^s\to 0$ as $z\to-\infty$. Since for $z\leqslant 0$, $\phi=0$, the boundary condition on the composition is $\phi=0$ at $z=0$.

To describe the time evolution of the film, dynamical equations for the fields $\mathbf{u}$, h and ϕ must be provided. These equations must represent the deposition process under consideration. For MBE, evaporation of particles from the film surface is neglected, and a constant amount of material is deposited per unit time. Hence, in a reference frame moving with the average surface position, the surface diffusion process must conserve the total amount of material. The material current at the surface is proportional to the gradient in the chemical potential

$$\mathbf{j}_h=-\Gamma_h\nabla\frac{\delta\mathcal{F}}{\delta h}, \tag{7}$$

where Γ_h is a kinetic coefficient. Because material is conserved, the time derivative of h is related to the divergence of the current, and h evolves as

$$\partial_t h=\Gamma_h\sqrt{g}\nabla_s^2\frac{\delta\mathcal{F}}{\delta h}+v, \tag{8}$$

where ∇_s^2 is the Laplace-Beltrami operator that ensures diffusion parallel to the surface, and v is the growth velocity.

The concentration field *at the surface* $\phi(x,y,t)=\phi(x,y,h(x,y),t)$ evolves in a similar manner,

$$\partial_t\phi=\Gamma_\phi\nabla_s^2\frac{\delta\mathcal{F}}{\delta\phi}-\Lambda\phi. \tag{9}$$

The very important last term in this equation represents the constant deposition of material of average composition equal

to 0, with Λ proportional to v. Since diffusion is neglected in the bulk, $\phi_b(x,y,z,t)=\phi(x,y,t=z/v)$. In principle, thermal and beam noises have to be included in Eqs. (8) and (9). Such effects, and a more detailed derivation of these equations, were described in a previous paper[3] and are not included here.

In the absence of elastic effects,[3] Eq. (8) becomes slaved to Eq. (9), and modulations of the surface arise due to the concentration gradients at the surface. This effect is nonlinear, however, and does not contribute to the linear stability.

The last evolution equation that has to be specified is for the field **u**. Since diffusion is a much slower process than local lattice rearrangements, the displacement vector can be taken to instantaneously satisfy mechanical equilibrium,

$$\nabla_j \sigma_{ij}=0. \tag{10}$$

These equations can be recast in terms of **u** once the stress tensor is specified. This will be described in the next section.

III. LINEAR STABILITY ANALYSIS

The linear stability analysis aims at calculating the growth rate of perturbations in the surface profile and in the concentration field. The procedure we describe here is similar to other calculations.[15,16] The reference state around which perturbations occur must be specified. The basic state for the surface consists of a planar growth front moving at a velocity v for the growing film, and of fixed thickness $\overline{h}$ for the static film. The substrate is unstrained and of lattice constant a_s, $\overline{\mathbf{u}^s}=0$, while the film is stressed in the x and y directions, such that the lattice constant in these directions is a_s. Since this is the reference state, $\overline{u_x}=\overline{u_y}=0$. Of course, the stress in the lateral directions will cause Poisson relaxation in the z direction, such that the compression $\nabla\cdot\overline{\mathbf{u}}=\overline{\mu_{zz}}$ is uniform, $\overline{u_z}=\overline{\mu_{zz}}z$, with the constant $\overline{\mu_{zz}}=[(1+\nu)/(1-\nu)]\varepsilon$. The stress in the lateral directions is then $\overline{\sigma}=-2\mu\overline{\mu_{zz}}$. We take the composition $\overline{\phi}$ of the initial state to be uniform and equal to zero. The general stress tensor, in the presence of misfit ε and compositional stresses, then reads[11,16]

$$\sigma_{ij}=2\mu\left[\frac{\nu}{1-2\nu}\mu_{ll}\delta_{ij}+\mu_{ij}-\frac{1+\nu}{1-2\nu}(\varepsilon+\eta\phi)\delta_{ij}\right]. \tag{11}$$

Substitution of this expression for the stress tensor in Eq. (10) leads to the mechanical equilibrium equations

$$\nabla_i\nabla\cdot\mathbf{u}+(1-2\nu)\nabla^2 u_i-2(1+\nu)\eta\nabla_i\phi=0. \tag{12}$$

The stability is studied by considering small perturbations around the basic state: a general variable ξ is expanded in a two-dimensional Fourier series as $\xi=\overline{\xi}+\Sigma_{\mathbf{q}}\hat{\xi}(\mathbf{q},z,t)e^{i(q_x x+q_y y)}$ (the Fourier coefficients for the height variable are independent of z). The functional derivative in Eq. (8), when computed, becomes the free-energy density evaluated at the surface. Hence, for the purpose of calculating $\partial_t\hat{h}$, the free-energy density has to be computed to $O(\hat{\xi})$. To this order, the Ginzburg-Landau free energy does not contribute, and we have the order $\hat{\xi}$ elastic energy $\hat{\mathcal{E}}$ as

$$\hat{\mathcal{E}}=\overline{\sigma}(\hat{\mu}_{xx}+\hat{\mu}_{yy}-2\eta\hat{\phi}). \tag{13}$$

For the dynamical equation for ϕ, the free-energy density must be computed to second order in the perturbations. Because of the mechanical equilibrium condition, the displacement vector can be obtained as a function of h and ϕ. The second-order correction to the elastic energy, $\tilde{\mathcal{E}}\sim O(\hat{\xi}^2)$, is

$$\tilde{\mathcal{E}}=S_{ijkl}\hat{\sigma}_{ij}\hat{\sigma}_{kl}. \tag{14}$$

A. Solutions of the mechanical equilibrium equations

The mechanical equilibrium equations are already linear and are, in the film,

$$(1-2\nu)(\partial_z^2-q^2)\hat{u}_x+iq_x(iq_x\hat{u}_x+iq_y\hat{u}_y+\partial_z\hat{u}_z-2(1+\nu)\eta\hat{\phi})=0, \tag{15}$$

$$(1-2\nu)(\partial_z^2-q^2)\hat{u}_y+iq_y(iq_x\hat{u}_x+iq_y\hat{u}_y+\partial_z\hat{u}_z-2(1+\nu)\eta\hat{\phi})=0, \tag{16}$$

$$(1-2\nu)(\partial_z^2-q^2)\hat{u}_z+\partial_z(iq_x\hat{u}_x+iq_y\hat{u}_y+\partial_z\hat{u}_z-2(1+\nu)\eta\hat{\phi})=0, \tag{17}$$

to first order. This is a set of coupled inhomogeneous second-order differential equations, with the inhomogeneity due to the concentration field. The homogeneous equations were derived by Spencer, Voorhees, and Davies,[15] while Guyer and Voorhees[16] obtained the full inhomogeneous set of equations. In the substrate, the displacements satisfy the homogeneous equations. The general solution to the inhomogeneous set is a linear combination of the solutions to the homogeneous problem added to the particular solution. The particular solution can easily be derived by taking an extra divergence in Eq. (12), leading to

$$u_i=\left(\frac{1+\nu}{1-\nu}\right)\eta\nabla_i W, \tag{18}$$

where W is defined through the relation

$$\nabla^2 W=\phi. \tag{19}$$

In the substrate, the displacements are

$$\begin{bmatrix}\hat{u}_x^s\\ \hat{u}_y^s\\ \hat{u}_z^s\end{bmatrix}=\begin{bmatrix}u_x^0\\ u_y^0\\ u_z^0\end{bmatrix}e^{qz}-\begin{bmatrix}iq_x/q\\ iq_y/q\\ 1\end{bmatrix}Bze^{qz}, \tag{20}$$

where $B=[1/(3-4\nu)](iq_x u_x^0+iq_y u_y^0+qu_z^0)$, and where we have used the condition that $\mathbf{u}^s$ vanishes far from the film/substrate boundary. In the film, we have

$$\begin{bmatrix} \hat{u}_x^f \\ \hat{u}_y^f \\ \hat{u}_z^f \end{bmatrix} = \begin{bmatrix} \alpha_x \\ \alpha_y \\ \alpha_z \end{bmatrix} \cosh(qz) + \begin{bmatrix} \beta_x \\ \beta_y \\ \beta_z \end{bmatrix} \sinh(qz) - \begin{bmatrix} Ciq_x/q \\ Ciq_y/q \\ D \end{bmatrix} z\sinh(qz) - \begin{bmatrix} Diq_x/q \\ Diq_y/q \\ C \end{bmatrix} z\cosh(qz) + \left(\frac{1+\nu}{1-\nu}\right)\eta \begin{bmatrix} iq_x\hat{W} \\ iq_y\hat{W} \\ \partial_z\hat{W} \end{bmatrix}. \tag{21}$$

In this last equation, C and D are defined as $C=[1/(3-4\nu)](iq_x\alpha_x+iq_y\alpha_y+q\beta_z)$ and $D=[1/(3-4\nu)](iq_x\beta_x+iq_y\beta_y+q\alpha_z)$. The above relations for the displacements in the film and in the substrate contain nine coefficients that have to be fixed using the boundary conditions. To $O(\hat{\xi})$, the boundary conditions are, at $z=h$,

$$\hat{\sigma}_{xz}=iq_x\overline{\sigma\hat{h}}, \quad \hat{\sigma}_{yz}=iq_y\overline{\sigma\hat{h}} \quad \text{and} \quad \hat{\sigma}_{zz}=0. \tag{22}$$

At $z=0$ to this order,

$$\hat{\sigma}_{zi}^f=\hat{\sigma}_{zi}^s \text{and } \hat{\mathbf{u}}^f=\hat{\mathbf{u}}^s. \tag{23}$$

The linearized boundary condition on ϕ is $\hat{\phi}=0$ at $z=0$, since we consider the alloy to be in the region $z>0$.

With these boundary conditions, we find that $u_i^0=\alpha_i=\beta_i$, which implies that $C=D=B$. For the energy calculation it is sufficient to specify C, as well as the relations between α_z and C:

$$C=A\left[-\frac{q\hat{h}\overline{\sigma}}{2\mu}+\eta\left(\frac{1+\nu}{1-\nu}\right)(q\partial_z\hat{W}-\partial_z^2\hat{W}+\hat{\phi})\Big|_{z=\overline{h}}\right], \tag{24}$$

$$q\alpha_z=C(2-2\nu+q\overline{h})+A\left[\frac{q\hat{h}\overline{\sigma}}{\mu}-2\eta\left(\frac{1+\nu}{1-\nu}\right)q\partial_z\hat{W}\Big|_{z=\overline{h}}\right], \tag{25}$$

where $A=[\cosh(q\overline{h})+\sinh(q\overline{h})]^{-1}$.

B. Calculation of the energy

The energy can now be calculated to second order in the perturbations from Eqs. (13) and (14),

$$\hat{\mathcal{E}}=\frac{E\varepsilon}{1-\nu}[-2\varepsilon(1+\nu)q\hat{h}-2\eta((1+\nu)q\partial_z\hat{W}-(1+\nu)\partial_z^2\hat{W}+\nu\hat{\phi})|_{z=\overline{h}}] \tag{26}$$

and

$$\begin{aligned}\tilde{\mathcal{E}}=\frac{E}{(1-2\nu)(1+\nu)}\Bigg[&(1-2\nu)\eta^2\hat{\phi}^2\left(\frac{1+\nu}{1-\nu}\right)\\&+2\varepsilon\left(\frac{1+\nu}{1-\nu}\right)q\hat{h}(1-2\nu)(1+\nu)\eta\hat{\phi}\\&+2(1-2\nu)\eta^2\left(\frac{1+\nu}{1-\nu}\right)^2\hat{\phi}[q\partial_z\hat{W}-\partial_z^2\hat{W}]\Big|_{z=\overline{h}}\\&+2(1-2\nu)(1-\nu)\eta^2\left(\frac{1+\nu}{1-\nu}\right)^2[q\partial_z\hat{W}-\partial_z^2\hat{W}]^2\Big|_{z=\overline{h}}\\&+8(1-2\nu)(1+\nu)\varepsilon\left(\frac{1+\nu}{1-\nu}\right)q\hat{h}\\&\times\eta[q\partial_z\hat{W}-\partial_z^2\hat{W}]\Big|_{z=\overline{h}}\Bigg].\end{aligned} \tag{27}$$

In this equation for $\tilde{\mathcal{E}}$, we have dropped terms of the form $\hat{h}^2$ because they do not contribute to the chemical potential for ϕ.

To obtain the function $\hat{W}$, we proceed as follows. We are interested in the early time regime where the fields grow exponentially in time, i.e., $\hat{\phi}=\hat{\phi}_0e^{\Omega t}$ and $\hat{h}=\hat{h}_0e^{\Omega t}$. This means that in the bulk of the film, $\hat{\phi}_b=\hat{\phi}_0e^{\Omega z/v}$, which gives, by Eq. (19),

$$\hat{W}=\frac{v^2\hat{\phi}_0}{\Omega^2-(qv)^2}e^{\Omega z/v}. \tag{28}$$

In particular, at the surface, $z=vt$, and $\hat{W}=v^2\hat{\phi}/[\Omega^2-(qv)^2]$, which implies that $\hat{\mathcal{E}}$ and $\tilde{\mathcal{E}}$ can be calculated in terms of $\hat{h}$ and $\hat{\phi}$ only. For completeness, we write these expressions here:

$$\hat{\mathcal{E}}=\frac{E\varepsilon}{1-\nu}\left[-2\varepsilon(1+\nu)q\hat{h}-2\eta\hat{\phi}\left(\frac{\nu qv-\Omega}{qv+\Omega}\right)\right] \tag{29}$$

and

$$\tilde{\mathcal{E}}=\frac{E}{1-\nu}\left\{\eta^2\hat{\phi}^2\left[1-2\left(\frac{1+\nu}{1-\nu}\right)\Omega\left(\frac{\nu\Omega+qv}{(\Omega+qv)^2}\right)\right]-2(1+\nu)\varepsilon\eta q\hat{h}\hat{\phi}\left(\frac{3\Omega-qv}{\Omega+qv}\right)\right\}. \tag{30}$$

C. Linearized dynamical equations

The dynamical equations for $\hat{h}$ and $\hat{\phi}$ are obtained from Eqs. (8) and (9). In Fourier space, they read

$$\partial_t\hat{h}=-\Gamma_h q^2\left(-2E\varepsilon^2\frac{1+\nu}{1-\nu}q\hat{h}-\frac{2E}{1-\nu}\varepsilon\eta\left(\frac{\nu qv-\Omega}{qv+\Omega}\right)\hat{\phi}+\gamma q^2\hat{h}\right) \tag{31}$$

and

$$\partial_t\hat{\phi}=-\Gamma_\phi q^2\left(-r'+cq^2+\frac{2E}{1-\nu}\eta^2\right)\hat{\phi}-\Gamma_\phi q^2\frac{4E}{1-\nu}\times\left[-\frac{1+\nu}{1-\nu}\left(\frac{\Omega}{\Omega+qv}\right)+(1+\nu)\left(\frac{\Omega}{\Omega+qv}\right)^2\right]\eta^2\hat{\phi}+\Gamma_\phi q^3 2E\frac{1+\nu}{1-\nu}\left(\frac{3\Omega-qv}{\Omega+qv}\right)\varepsilon\,\eta\hat{h}-\Lambda\hat{\phi}. \tag{32}$$

It can be seen from these equations that the two variables are coupled due to the elastic effects. In Eq. (32), the term $[2E/(1-\nu)]\eta^2\hat{\phi}$ simply renormalizes the coefficient r' and was first calculated by Cahn[17] in the case of a bulk binary mixture. Experimentally, only the renormalized value for r' is accessible, and we therefore introduce a new coefficient $r=r'-2E\eta^2/(1-\nu)$, which is proportional to $T_c^{\rm eff}-T$, and we consider the cases where T is above and below $T_c^{\rm eff}$.

The dynamical equations can be rescaled using typical length and time scales. We take the typical width of interfaces between domains as the length scale, and make the transformation $\mathbf{x}=(|r|/c)^{1/2}\mathbf{r}$ and $k=(c/|r|)^{1/2}q$. Note that when the constants Γ_h and v are rescaled by this length scale, they become equivalent to Γ_ϕ and Λ [see discussions around Eqs. (7)–(9)]. The time scale is then related to the surface diffusion constant Γ_ϕ, leading to the rescaling $\tau=(\Gamma_\phi r^2/c)t$. We also introduce new parameters ε^*, η^*, and γ^* defined as

$$\varepsilon^*=\left[\frac{2E}{|r|}\left(\frac{1+\nu}{1-\nu}\right)\right]^{1/2}\varepsilon, \tag{33}$$

$$\eta^*=\left[\frac{2E}{|r|}\left(\frac{1+\nu}{1-\nu}\right)\right]^{1/2}\eta, \tag{34}$$

and

$$\gamma^*=(c|r|)^{-1/2}\gamma. \tag{35}$$

Furthermore, the growth parameter is also rescaled,

$$V=\left(\Gamma_\phi\frac{r^2}{c}\right)^{-1}\Lambda, \tag{36}$$

while the dimensionless dispersion is

$$\sigma=\left(\Gamma_\phi\frac{r^2}{c}\right)^{-1}\Omega. \tag{37}$$

For most semiconductor materials, the Poisson ratio varies around a value of 1/4. For this value of ν, the dimensionless dynamical equations are ($\hat{h}$ has also been rescaled)

$$\partial_\tau\hat{h}=-k^2\left[-\varepsilon^{*2}k\hat{h}-\frac{1}{5}\varepsilon^*\eta^*\left(\frac{kV-4\sigma}{kV+\sigma}\right)\hat{\phi}+\gamma^*k^2\hat{h}\right] \tag{38}$$

and

$$\partial_\tau\hat{\phi}=-k^2\left(\pm1+k^2+\frac{V}{k^2}-\frac{2}{3}\eta^{*2}\sigma\frac{\sigma+4kV}{(\sigma+kV)^2}\right)\hat{\phi}+k^3\varepsilon^*\eta^*\left(\frac{3\sigma-kV}{\sigma+kV}\right)\hat{h}. \tag{39}$$

In Eq. (39) [and Eqs. (40), (42), (44), (45), and (46) below], the top sign is taken if the alloy is above the critical temperature and the bottom sign applies if the alloy is below the critical temperature. Immediate important conclusions can be drawn from these equations. In a general case where none of the parameters vanish, the morphological and compositional degrees of freedom are always coupled. Thus, if one of the variables is unstable, then the other will also be unstable. Therefore, decomposition of the alloy will always be accompanied by a surface instability, and the only way a planar surface can be stabilized is if spinodal decomposition is suppressed. In the same way, if a misfit drives a surface instability, it will induce phase separation at the surface. In general, for $T<T_c$, both the instability due to the misfit and the thermodynamic instability of the alloy are present, and the system evolves with a single dispersion relation that is a combination of the two instabilities. The second important conclusion is concerned with the signs of the misfit ε^* and of the solute expansion coefficient η^*. It can be seen in Eqs. (38) and (39) that ε^*, and η^* appear only in the combinations ε^{*2}, η^{*2}, and $\varepsilon^*\eta^*$, implying that the only possible dependence on the signs of ε^* and η^* would be from the $\varepsilon^*\eta^*$ terms, i.e., the *coupling* terms in the equations. Consider, for instance, the term proportional to $\hat{\phi}$ in Eq. (38). To replace the fluctuation in $\hat{\phi}$ by a function of $\hat{h}$, one has to first (simultaneously) solve Eq. (39), giving $\hat{\phi}\sim\varepsilon^*\eta^*\hat{h}$, which is then substituted back in Eq. (38), yielding an effective contribution which is proportional to $(\varepsilon^*\eta^*)^2$. Hence, the stability is *independent* of the sign of the misfit or the expansion coefficient.

To solve for the dispersion relation, we let $\hat{h}=\hat{h}_0e^{\sigma\tau}$, $\hat{\phi}=\hat{\phi}_0e^{\sigma\tau}$ and require that the determinant of the matrix formed by the equations for $\hat{h}_0$ and $\hat{\phi}_0$ be equal to zero. We find that σ satisfies the quartic equation,

$$0=\left\{[\sigma+k^2(k^2\pm1)+V](\sigma+kV)^2-\tfrac{2}{3}\eta^{*2}k^2\sigma(\sigma+4kV)\right\}[\sigma+\gamma^*k^4-\varepsilon^{*2}k^3]+\tfrac{1}{5}k^5(\varepsilon^*\eta^*)^2(3\sigma-kV)(4\sigma-kV). \tag{40}$$

It can now easily be seen that σ does not depend on the sign of ε^* or η^*. In general, there exist four complex solutions to Eq. (40). The real part of σ determines the stability of the system, while the presence of a nonzero imaginary part for σ is responsible for oscillations. Here, we are only interested in the stability of the system, and concentrate on the real part of σ. When the analytical solutions for σ are complicated we proceed numerically, and for a given value of k, we calculate the real part of each of the four solutions, and denote the largest of these four values as σ. Hence, below, when we indicate $\sigma>0$, it means that the real part of at least one of the four roots is positive, leading to an instability, and σ represents the most unstable dispersion.

IV. RESULTS FOR STATIC FILMS

In the case of a static film of fixed average height, the expression for $\hat{W}$ in Eq. (28) is no longer valid. In principle, Eq. (19) has to be solved for a composition given by a δ function in $z-h$. However, a simpler argument is as follows: if we assume that $\hat{\phi}_b = \hat{\phi}_s e^{-\lambda(z-h)}$ where $\hat{\phi}_s$ is the value of the order parameter at the surface, then $\hat{W}$ is easily calculated. Substitution of the expression for $\hat{W}$ in the elastic energy Eq. (27) and taking the limit $\lambda \gg q$ yields the same result as setting *the growth velocity V to zero*. The expression for $\hat{\phi}_b$ above is similar in spirit to the calculations of Glas for an equilibrium static film.[18] Various scenarios are possible depending on the values of ε^* and η^*. When both ε^* and η^* are zero (i.e., a film perfectly matched to the substrate and with the lattice constant independent of composition), the dynamical equations decouple and there are two nontrivial solutions for σ. For the height variable,

$$\sigma_h = -\gamma^* k^4, \tag{41}$$

which is always negative, leading to a stable planar surface. For the compositional degree of freedom, we have

$$\sigma_\phi = -k^4 \mp k^2, \tag{42}$$

which is positive in the band of wave vectors $0<k<1$ for $T<T_c$, and is always negative for $T>T_c$. When $T<T_c$, σ_ϕ is the usual expression for spinodal decomposition of a symmetric binary alloy, and in the absence of nonlinear elastic effects, complete phase separation of the two components results. The most unstable wave vector is $k_m^\phi = 1/\sqrt{2}$, and $\sigma_\phi(k_m^\phi) = 1/4$. We plot σ_h and σ_ϕ in Fig. 1(a) for $T<T_c$.

When only the substrate misfit is present ($\varepsilon^* \neq 0, \eta^* = 0$), the equations are still decoupled, and we recover the result of Asaro and Tiller for the surface dispersion,

$$\sigma_h = \varepsilon^{*2} k^3 - \gamma^* k^4. \tag{43}$$

The misfit induces a surface instability, since σ_h is positive in the region $0<k<\varepsilon^{*2}/\gamma^*$, with the maximum in the dispersion at $k_m^h = (3/4)\varepsilon^{*2}/\gamma^*$, and $\sigma_h(k_m^h) = (27/256)\varepsilon^{*8}/\gamma^{*3}$. The dispersion for ϕ is the same as Eq. (42) [see Fig. 1(b)].

In the absence of a misfit but in the presence of a nonzero solute expansion coefficient ($\varepsilon^*=0$, $\eta^* \neq 0$), the two variables are decoupled and the surface is always stable, since its dispersion is given by Eq. (41). For the composition, the dispersion is given by

$$\sigma_\phi = -k^4 + k^2\left(\mp 1 + \tfrac{2}{3}\eta^{*2}\right). \tag{44}$$

Below T_c, the dispersion is now positive in $0<k<\sqrt{1+(2/3)\eta^{*2}}$, with a maximum at $k_m^\phi = (1/\sqrt{2})(1+(2/3)\eta^{*2})^{1/2}$. The value of the dispersion relation at the maximum is increased to $\sigma_\phi(k_m^\phi) = (1/4)(1+(2/3)\eta^{*2})^2$, implying that the contribution due to η^{*2} increases the instability to phase separation as well as the value of the most unstable wave vector [Fig. 1(c)]. Above T_c, the elastic fields can induce a decomposition of the alloy since σ_ϕ can become positive if $\eta^{*2} > 3/2$. The extra term $(2/3)\eta^{*2}$ in Eq. (44) originates from the elastic fields generated by composition inhomogeneities at the surface that are constrained by the boundary condition on the stress tensor at the surface, and corresponds to the third and fourth terms proportional to η^{*2} in Eq. (27).

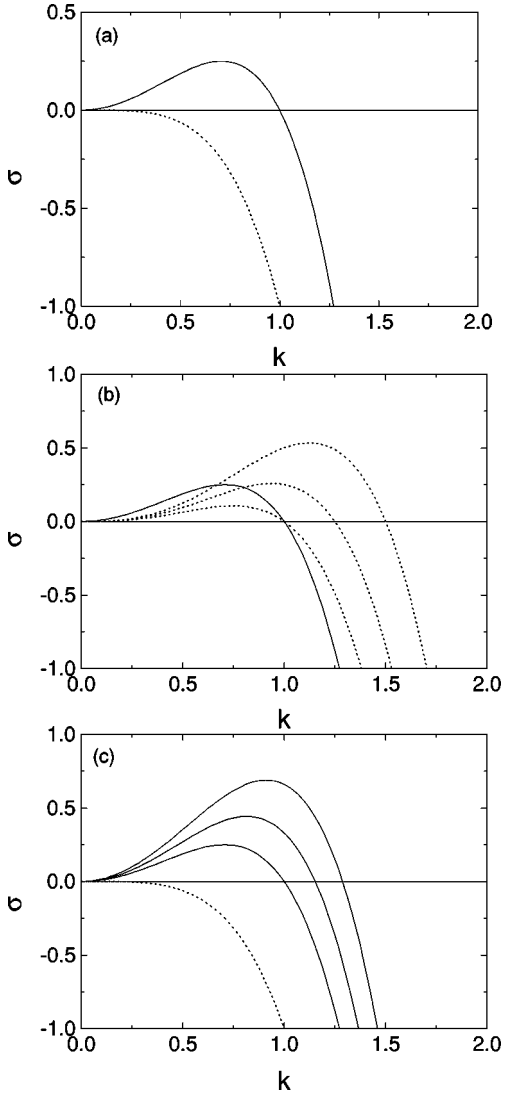

FIG. 1. Dispersion relations when the morphological and compositional degrees of freedom decouple. The solid lines represent the dispersion for ϕ when $T<T_c$, while the dotted lines are for h. The parameter $\gamma^*=1$. In (a), $\varepsilon^*=\eta^*=0$. In (b), $\eta^*=0$, and the dotted curves from bottom to top are for $\varepsilon^*=1$, 1.25, and 1.5. In (c), $\varepsilon^*=0$, and the solid lines from bottom to top correspond to $\eta^*=0$, 0.5, and 1.

The most interesting case for a static film corresponds to a compositionally stressed film on a mismatched substrate, because the dynamical equations are coupled due to the terms proportional to $\varepsilon^* \eta^*$. Because the variables are coupled, the dispersion relation describes the stability of both variables simultaneously. We first describe the results for $T<T_c$. In Fig. 2, we plot the maximum of the real part of the dispersion relations for a fixed value of ε^* but for different values of η^*. As can be seen in this figure, σ is always positive in a band of wave vectors and has two peaks: the first peak at lower k is due to η^*, while the second peak is due to the misfit ε^*. As η^* is increased, the value of σ at the first peak increases and the peak location moves to a larger k value. Eventually, for very large η^* (not shown in the figure), the

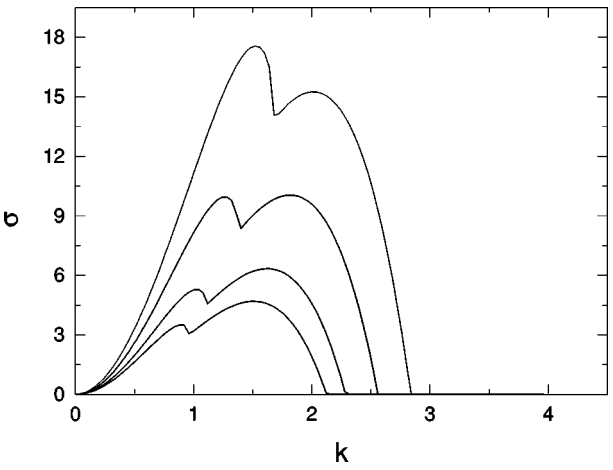

FIG. 2. Dispersion relation for the static film when h and ϕ are coupled for $T<T_c$. The misfit $\varepsilon^*=0.75$ and $\eta^*=3.2$, 3.5, 4, and 4.5 from bottom to top.

first peak is so strong that only one peak is apparent. Except for a special case, one of the peaks will be larger than the other, and the most unstable wave vector will come from that peak. In the special case where the two peaks have the same height, the surface becomes most unstable at two wave vectors simultaneously.

When the temperature is above the critical temperature, there is a region of stability that appears in the $\varepsilon^*-\eta^*$ diagram, as shown in Fig. 3. It can be seen that if η^* or ε^* are too large the coupled system is always unstable. The shape of the stability diagram implies that if the misfit is moderate, the system can be stabilized due to the elastic fields generated by the composition; if the value of η^* is not large enough, the amplitude of the compositional stresses will not be sufficient to control the instability due to the misfit. The results of the stability analysis for the static film are summarized in Table I.

In their study, Guyer and Voorhees[16] find that for the static film, compositional strain plays no role in the instability. This is because, in their model, composition decouples

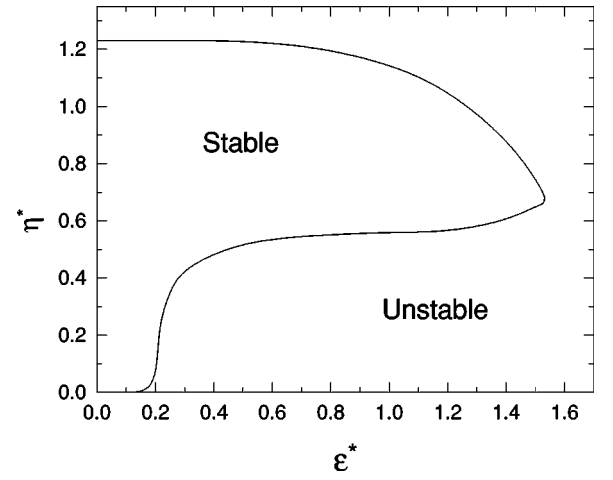

FIG. 3. Stability diagram for the static film grown above the critical temperature. A joint instability occurs in the unstable region and a joint stability occurs in the stable region. The surface constant $\gamma^*=1$.

TABLE I. Summary of the stability results for the static film.

Temperature	ε^*	η^*	Surface	Alloy
$T<T_c$	0	0	stable	unstable
	0	$\neq 0$	stable	unstable
	$\neq 0$	0	unstable	unstable
	$\neq 0$	$\neq 0$	joint instability	joint instability
$T>T_c$	0	0	stable	stable
	0	$\neq 0$	stable	stable if $\eta<\eta_c$
	$\neq 0$	0	unstable	stable
	$\neq 0$	$\neq 0$	see Fig. 3	see Fig. 3

from the elastic field and implies $\partial_t\phi=0$. We believe that by appropriately including the nonequilibrium evolution of ϕ we have captured the missing ingredient to make the understanding of the problem more consistent. Glas[18] has recently calculated the equilibrium stability (in the sense of thermodynamics) of an alloy in a planar half-space the surface of which is allowed to deviate from planarity. There, it is found that the state that minimizes the energy consists of a joint modulation of the composition and of the free surface, even if the alloy is stable against decomposition in bulk form. The dynamical analysis presented in the present paper suggests that the equilibrium state may not always be kinetically accessible since there exist combinations of the misfit, the solute expansion coefficient, and the temperature for which stabilization occurs.

V. RESULTS FOR GROWING FILMS

When the film is growing, the growth parameter V becomes important in determining the stability. Again, when $\varepsilon^*=0$ or $\eta^*=0$, the dynamical equations for h and ϕ decouple and each variable has its own dispersion relation; in the general case where both ε^* and η^* are nonzero, the variables are coupled and their time evolution is governed by the same dispersion relation.

To establish basic results, we start by describing a perfectly matched film where its constituents are of the same size ($\varepsilon^*=\eta^*=0$). Here, the surface is always stable, since there are no compositionally generated stresses and no misfit. The dispersion relation for h is given by Eq. (41). Because there is a competition between the constant deposition of material of fixed average composition and the formation of phase separated domains at the surface, the growth rate V can be used to stabilize the homogeneous mixture. This can be seen in the dispersion relation for ϕ, which reads

$$\sigma_\phi=-k^4\mp k^2-V. \tag{45}$$

For the positive sign, the dispersion relation is positive in the band $1-\sqrt{1-4V}<2k^2<1+\sqrt{1-4V}$, provided that the growth rate $V<1/4$. Hence, if $V>1/4$, the constant deposition is too strong for the phase separation, and the alloy is stabilized against decomposition. This implies that there exists a critical growth rate V_c above which the film will be homogeneous in composition. When the growth parameter is below 1/4,[4] a top view of the system shows lamellar or droplet concentration patterns in the steady state. The appearance of droplets is due to nonlinear elastic effects that favor the

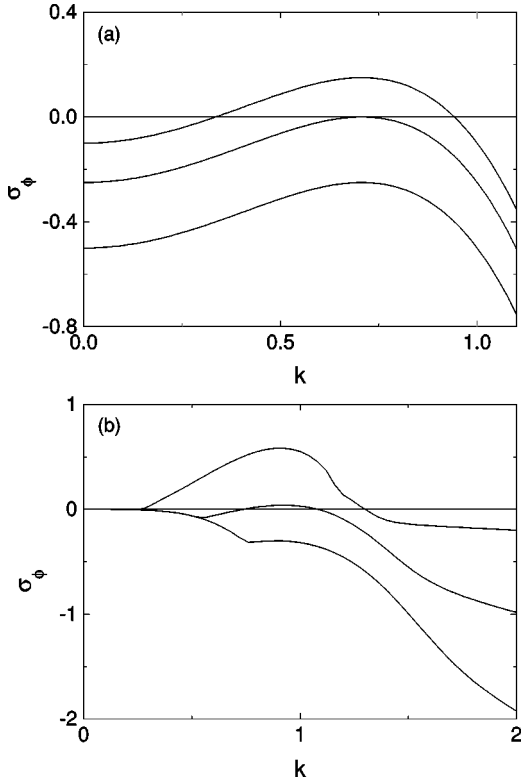

FIG. 4. Dispersion relation for ϕ in the case of the uncoupled growing film when $T<T_c$. In (a), we plot the dispersion relation when $\eta^*=\varepsilon^*=0$ for (bottom to top) $V=0.5$, 0.25, and 0.1. In (b), $\eta^*=1$, $\varepsilon^*=0$, and the curves from bottom to top correspond to $V=1$, 0.5, and 0.1.

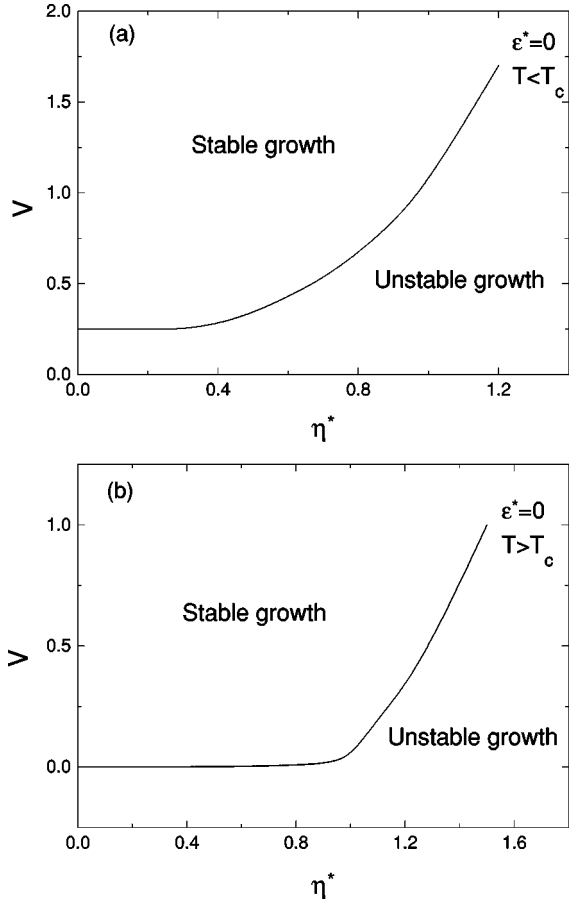

FIG. 5. Critical growth rate as a function of the solute expansion coefficient for (a) $T<T_c$ and (b) $T>T_c$. For $V>V_c$ the system is stable.

formation of hard droplets in a soft matrix. We plot σ_ϕ in Fig. 4(a). For the negative sign, the alloy is always stable against decomposition.

If the film is mismatched but $\eta^*=0$, the surface is unstable due to the Asaro and Tiller instability and its dispersion is given by Eq. (43), while the composition is unaffected by the misfit and Eq. (45) is still valid. The most unstable wave vectors are in general different for the instabilities in h and ϕ, which means that at early times, the size of concentration domains will be uncorrelated to the size of surface perturbations.

The surface of a matched film ($\varepsilon^*=0$) in the presence of both the deposition process and the compositional stresses is always stable, since $\sigma_h=-\gamma^* k^4$. The stability around the average composition is described by the solutions to a cubic equation in σ_ϕ,

$$[\sigma_\phi+k^2(k^2\pm 1)+V](\sigma_\phi+kV)^2 - \tfrac{2}{3}k^2\eta^{*2}\sigma_\phi(\sigma_\phi+4kV)=0. \quad (46)$$

In Fig. 4(b), we plot σ_ϕ as a function of k for different values of V and η^* for temperatures inside of the miscibility gap. As can be seen in this figure, the band of wave vectors where σ_ϕ is positive decreases in size as V is increased. For V large enough, σ_ϕ is always negative, implying that the homogeneous alloy is stable. The critical growth rate introduced earlier now depends on η^* as shown in Fig. 5. As an indication, we find that fot $T<T_c$, V_c increases roughly as η^{*2} over the range plotted [Fig. 5(a)]. For temperatures outside of the miscibility gap, there is a range of η^*, $0<\eta^*<1$ where the alloy is stable at any growth rate [Fig. 5(b)]. Note that when $\varepsilon^*=0$ and $\eta^*=0$ the alloy is always stable against decomposition [see Eq. (45)]. If $\eta^*>1$ and $T>T_c$, spinodal decomposition occurs at low growth rates and is suppressed at high growth rates, as shown in Fig. 5(b).

For most situations, none of the parameters vanish, and the two variables are always coupled. In Fig. 6, we plot σ as a function of the wave-vector amplitude for various combinations of the parameters ε^*, η^* and V for $T<T_c$. In Fig. 6(a), we plot σ for fixed values of ε^* and η^* but for different growth velocities, showing that as V is increased, σ becomes negative for all k when $V>V_c$. Note however, that the location of the maximum does not change much with V. If V and ε^* are fixed while η^* is increased [Fig. 6(b)], the coupled system goes from stable to unstable, and the location of the maximum increases with η^* as discussed in previous cases. The effects of the misfit ε^* on the stability are shown in Fig. 6(c). There is a maximum value for $\varepsilon^*, \varepsilon^*_{\max}$ above which the system is unstable. Below this maximum misfit, the deposition is strong enough to control the compositional gradients generated by the intrinsic phase separation and by the surface instability, but as the misfit is increased the instability driven by ε^* becomes stronger than the deposition. The value of $\varepsilon^*_{\max}$ depends only on the surface tension γ^*: $\varepsilon^*_{\max}\sim\gamma^{*1/2}$. In Fig. 7, we plot a stability diagram for the coupled system, showing the stable and unstable regions.

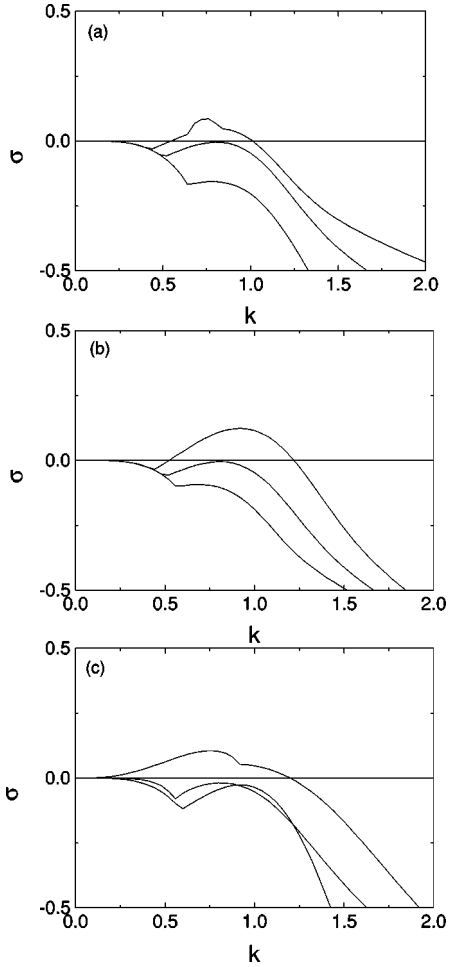

FIG. 6. Dispersion relation for the growing film when h and ϕ are coupled when $T<T_c$. (a) $\varepsilon^*=0.1$, $\eta^*=0.5$. From bottom to top: $V=0.6$, 0.34, and 0.25. (b) $\varepsilon^*=0.1$, $V=0.34$. From bottom to top: $\eta^*=0.25$, 0.5, and 0.75. (c) $\eta^*=0.5$, $V=0.4$. From bottom to top: $\varepsilon^*=0.1$, 0.5, and 1.

The shape of the stability diagram is generic for the alloy grown either above or below the critical temperature since we find that the maximum misfit is independent of whether T is above or below T_c and the critical velocity boundary is horizontal in both cases. The stability diagram can be interpreted for any value of the temperature if the the value of the threshold velocity is taken from Fig. 5. A summary of our results is presented in Table II. From a step-flow growth model, Tersoff[12] concluded that alloy decomposition can never stabilize a growing mismatched surface, independently of the sign of the misfit. Our work indicates that stabilization is possible by appropriately choosing the growth rate, since the constant deposition of material competes with the alloy decomposition. Furthermore, the results for the static films presented in this paper follow naturally from our general model for the growing alloy by taking the limit of zero growth rate, in contrast to the step-flow model[12] which is inapplicable as $V\rightarrow 0$.

VI. COMPOSITION-DEPENDENT YOUNG'S MODULUS

In this section, we extend the calculations above to include a linear dependence of Young's modulus on the order

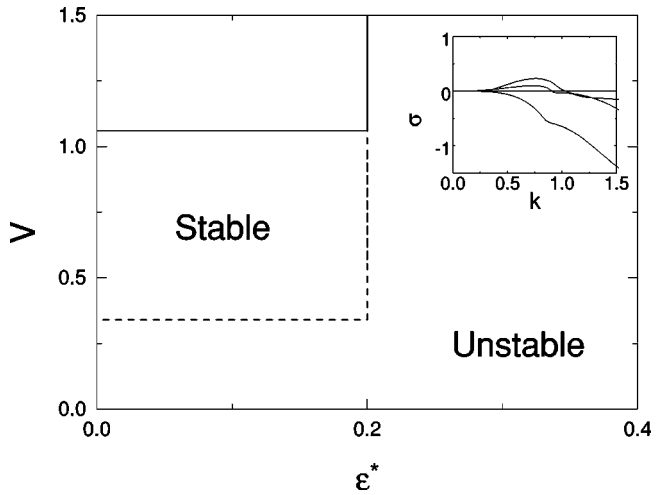

FIG. 7. Stability diagram for the growing film when $\gamma^*=1$ and for composition-independent elastic moduli when $T<T_c$. The dashed (solid) lines are for $\eta^*=0.5$ ($\eta^*=1$). The vertical solid and dashed lines overlap for $V>1.06$. The inset shows the dispersion relation for different values of the misfit and the growth rate for $\eta^*=0.5$. Bottom to top: $(\varepsilon^*,V)=(0.1, 0.5)$, (0.1, 0.2), and (0.3, 0.5). The stability diagram can be interpreted for $T>T_c$ if the threshold growth rate is taken from Fig. 5.

parameter. We write $E=E_0+E_1\phi$ and assume that the shear modulus is constant, $\mu=\mu_0$. Taking E and μ as the two independent elastic moduli, the Poisson ratio is $\nu=\nu_0+\nu_1\phi$ with $\nu_0=(E_0-2\mu_0)/(2\mu_0)$ and $\nu_1=(E_1/E_0)(1+\nu_0)$. The first-order stress tensor is

$$\hat{\sigma}_{ij}=2\mu_0\left[\left(\frac{\nu_0}{1-2\nu_0}\right)\hat{\mu}_{ll}\delta_{ij}+\hat{\mu}_{ij}-\frac{1+\nu_0}{1-2\nu_0}\theta\hat{\phi}\delta_{ij}\right], \tag{47}$$

with $\theta=\eta+2(E_1/E_0)\varepsilon/(1-\nu_0)$ a new effective solute expansion coefficient. The elastic energy is now

$$\hat{\mathcal{E}}=\overline{\sigma}(\hat{\mu}_{xx}+\hat{\mu}_{yy}-2[\eta-(E_1/E_0)\varepsilon/(1-\nu_0)]\hat{\phi}) \tag{48}$$

and

$$\tilde{\mathcal{E}}=\overline{S}_{ijkl}\hat{\sigma}_{ij}\hat{\sigma}_{kl}+\hat{S}_{ijkl}\overline{\sigma_{ij}}\hat{\sigma}_{kl}. \tag{49}$$

Elimination of the displacement vector through the mechanical equilibrium equations leads to (to first order in E_1)

TABLE II. Summary of the stability results for the growing film.

Temperature	ε^*	η^*	Surface	Alloy
$T<T_c$	0	0	stable	stable if $V>V_c$
	0	$\neq 0$	stable	stable if $V>V_c(\eta)$
	$\neq 0$	0	unstable	stable if $V>V_c$
	$\neq 0$	$\neq 0$	see Fig. 7	see Fig. 7
$T>T_c$	0	0	stable	stable
	0	$\neq 0$	stable	stable if $V>V_c(\eta)$
	$\neq 0$	0	unstable	stable
	$\neq 0$	$\neq 0$	see Fig. 7	see Fig. 7

$$\hat{\mathcal{E}}=\frac{E_0\varepsilon}{1-\nu_0}\left\{-2\varepsilon(1+\nu_0)q\hat{h}-2\left[\theta\left(\frac{\nu_0 qv-\Omega}{qv+\Omega}\right)-\frac{E_1}{E_0}\frac{\varepsilon}{1-\nu_0}\right]\hat{\phi}\right\} \tag{50}$$

and

$$\begin{aligned}\tilde{\mathcal{E}}=&\frac{E_0}{1-\nu_0}\left\{\left(\eta^2+4\varepsilon\eta\frac{E_1}{E_0}\right)\right.\\&\times\left[1-2\left(\frac{1+\nu_0}{1-\nu_0}\right)\Omega\left(\frac{\nu\Omega+qv}{(\Omega+qv)^2}\right)\right]\hat{\phi}^2\\&+\frac{4\varepsilon\eta}{1-\nu_0}\frac{E_1}{E_0}\left(\frac{\nu_0 qv-\Omega}{qv+\Omega}\right)\hat{\phi}^2+q\hat{h}\hat{\phi}\left[\left(-2\varepsilon\eta(1+\nu_0)\right.\right.\\&\left.\left.-4\varepsilon^2\frac{E_1}{E_0}\frac{1+\nu_0}{1-\nu_0}\right)\left(\frac{3\Omega-qv}{\Omega+qv}\right)+4\varepsilon^2\frac{E_1}{E_0}\frac{1+\nu_0}{1-\nu_0}\right]\Bigg\}.\end{aligned} \tag{51}$$

For $\nu_0=1/4$, the rescaled dynamical equations are ($E_1^*=E_1/E_0$and $T<T_c$)

$$\partial_\tau\hat{h}=-k^2\left\{-\varepsilon^{*2}k\hat{h}-\left[\frac{1}{5}\varepsilon^*\eta^*\left(\frac{kV-4\sigma}{kV+\sigma}\right)+\frac{2}{5}E_1^*\varepsilon^{*2}\left(\frac{3kV-2\sigma}{kV+\sigma}\right)\right]\hat{\phi}+\gamma^*k^2\hat{h}\right\} \tag{52}$$

and

$$\begin{aligned}\partial_\tau\hat{\phi}=&-k^2\left[-1+k^2+\frac{V}{k^2}\right.\\&-\frac{2}{3}(\eta^{*2}+4\varepsilon^*\eta^*E_1^*)\sigma\frac{\sigma+4kV}{(\sigma+kV)^2}\\&\left.+\frac{32}{15}\varepsilon^*\eta^*E_1^*\left(\frac{kV-\sigma}{kV+\sigma}\right)\right]\hat{\phi}+k^3\left[\left(\varepsilon^*\eta^*+\frac{8}{3}E_1^*\varepsilon^{*2}\right)\right.\\&\left.\times\left(\frac{3\sigma-kV}{\sigma+kV}\right)-\frac{8}{3}E_1^*\varepsilon^{*2}\right]\hat{h}.\end{aligned} \tag{53}$$

It can be seen in these equations that the composition dependence of E introduces nontrivial dynamical terms and a dependence on the sign of the misfit ε^*. The dependence on the sign of ε^* can be understood as follows: for example, a film under compression with $\eta^*>0$ would be less unstable for $E_1^*<0$ since the larger atoms are easier to compress. It can also be noted that even in the absence of η^* the variables are coupled due to the terms in E_1^*. The new stability diagram for the growing film is presented in Fig. 8, showing that the maximum misfit is still present and the asymmetry when the sign of the misfit is reversed.

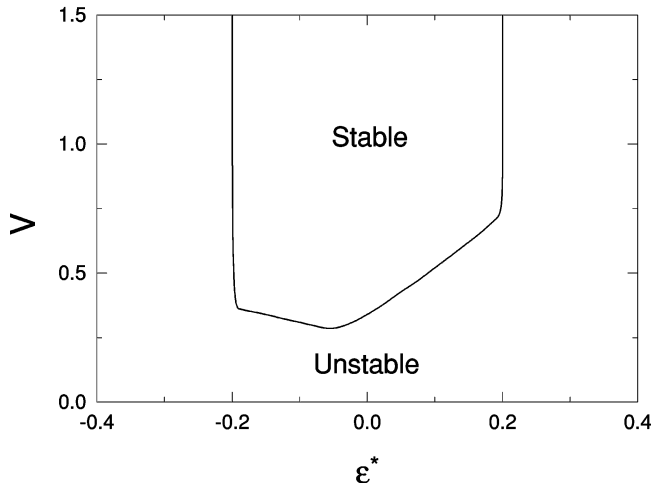

FIG. 8. Stability diagram for the growing film when $\gamma^*=1$ with a composition-dependent Young's modulus ($E_1^*=1$, $\eta^*=0.5$ and $T<T_c$).

VII. CONCLUSION

In this paper, we have shown that a proper description of static or growing solid films requires considerations of the nonequilibrium nature of the surface diffusion. We obtained coupled dynamical equations for the local composition of the alloy and for the surface profile. The most important conclusion in our work is that, in general, the composition and surface height variables are coupled, implying that a film with a stable (unstable) planar surface is also stable (unstable) against decomposition of the alloy. Another important conclusion is the fact that the stability is independent of the sign of the mismatch between the film and the substrate when the elastic moduli are independent of composition. This symmetry can be broken if the Young's modulus of the alloy constituents depends on composition. A planar film with the appearance of modulations perpendicular to the growth direction can be obtained if the film is perfectly matched to the substrate. For the unstable surfaces, our calculations suggest that the mode with the most unstable wave number will grow faster. However, this does not necessarily mean that a film of arbitrary thickness will show modulations of wave number q_m. In fact, nonlinear effects become important on a thickness scale $V\sigma_m^{-1}$, where a possible crossover from q_m to a steady-state wave number can occur. Of course, the large stress concentrations at this point may also lead to the formation of dislocations.

ACKNOWLEDGMENTS

This work was supported by the NSERC of Canada. F.L. also acknowledges support from the Walter C. Sumner Fund.

[1] A. Zunger and S. Mahajan, *Handbook on Semiconductors*, 2nd ed. (Elsevier, Amsterdam, 1993), Vol. 3.
[2] F. Léonard, M. Laradji, and R. C. Desai, Phys. Rev. B **55**, 1887 (1997).
[3] F. Léonard and R. C. Desai, Phys. Rev. B **55**, 9990 (1997).
[4] F. Léonard and R. C. Desai, Phys. Rev. B **56**, 4955 (1997).
[5] D. E. Jesson, S. J. Pennycook, J.-M. Baribeau, and D. C. Houghton, Phys. Rev. Lett. **71**, 1744 (1993).
[6] C. W. Snyder, B. G. Orr, D. Kessler, and L. M. Sander, Phys. Rev. Lett. **66**, 3032 (1991).
[7] F. K. Legoues, M. Copel, and R. M. Tromp, Phys. Rev. B **42**, 11 690 (1990).
[8] R. J. Asaro and W. A. Tiller, Metall. Trans. A **3**, 1789 (1972).
[9] D. J. Srolovitz, Acta Metall. **37**, 621 (1989).
[10] B. J. Spencer, P. W. Voorhees, and S. H. Davies, Phys. Rev. Lett. **26**, 3696 (1991).
[11] J. E. Guyer and P. W. Voorhees, Phys. Rev. Lett. **20**, 4031 (1995).
[12] J. Tersoff, Phys. Rev. Lett. **77**, 2017 (1996).
[13] T. Walther, C. J. Humphreys, and A. G. Cullis, Appl. Phys. Lett. **71**, 809 (1997).
[14] T. Okada, G. C. Weatherly, and D. W. McComb, J. Appl. Phys. **81**, 2185 (1997).
[15] B. J. Spencer, P. W. Voorhees, and S. H. Davies, J. Appl. Phys. **73**, 4955 (1993).
[16] J. E. Guyer and P. W. Voorhees, Phys. Rev. B **54**, 11 710 (1996).
[17] J. W. Cahn, Acta Metall. **9**, 795 (1961).
[18] F. Glas, Phys. Rev. B **55**, 11 277 (1997).